# High sensitivity side-hole fiber magnetic field sensor based on surface plasmon resonance

**Sijun Weng (翁思俊), Li Pei (裴 丽)*, Jianshuai Wang (王建帅), Tigang Ning (宁提纲), and Jing Li (李 晶)**

*Key Lab of All Optical Network and Advanced Telecommunication Network of Ministry of Education, Institute of Lightwave Technology, Beijing Jiaotong University, Beijing 100044, China*

**Corresponding author: lipei@bjtu.edu.cn*

Received July 22, 2016; accepted September 23, 2016; posted online October 21, 2016

A high sensitivity magnetic fluid (MF) filled side-hole fiber magnetic field sensor based on surface plasmon resonance (SPR) is designed and investigated. Within the side-hole fiber, the water-based MF is injected into the two side holes, and both of the holes are coated with gold to realize the measurement of the magnetic field by using the SPR effect. The refractive index of the MF changes with different external magnetic fields, resulting in the resonant wavelength moving to other wavelengths. Furthermore, when the external magnetic field increases from 30 to 210.9 Oe, the magnetic field sensitivity can reach to 1.063 nm/Oe.

*OCIS codes: 240.6680, 060.2370, 160.3820.*
*doi: 10.3788/COL201614.110603.*

Fiber magnetic field sensors have attracted more and more attention due to the advantages of electromagnetic wave immunity, real time monitoring, small size, and so on. Moreover, with the development of nanotechnology, magnetic materials become one of the most important components for the measurement of the magnetic field. As one kind of magnetic material, magnetic fluid (MF) is a colloid which contains of suitable liquid carrier and magnetic nanoparticle. It can be classified as water-based, oil-based, and ester-based MF based on the different liquid carriers[1]. As one of the characteristics, when the external magnetic field applies to the MF, the refractive index is changed because of the magnetic-optical effect. Combining with fibers, there are some kinds of MF fiber sensors[2–5]. Miao *et al.* have theoretically and experimentally investigated a magnetic field tunable fiber sensor based on an S-tapered microfiber[6]. Zu *et al.* designed a magnetic field sensor, which is configured as a Sagnac interferometer structure and a MF film. The output spectrum of the Sagnac interferometer moves to the other wavelength when the strength of the applied magnetic field is changed, obtaining the magnetic field sensitivity of 16.7 pm/Oe[7]. Moreover, Chen *et al.* investigated the sensing characteristic of a single mode–multimode–single mode (SMS) fiber structure with the sensitivity of 905 pm/mT[8]. For the liquid characteristic, the MF can be filled into the photonic crystal fiber (PCF) to realize the magnetic field measurement. Li *et al.* have proposed a magnetic field dual-core PCF sensor by filling MF into air holes[9]. A magnetic field sensor with the sensitivity of 242 pm/mT has been reported by Thakur *et al.*, in which the $Fe_3O_4$ magnetic nano-fluid is injected into the cladding holes of the polarization-maintaining PCF[10]. However, the PCF sensor has a problem on the connection of a single mode fiber and the PCF.

Alternatively, the surface plasmon resonance (SPR) also can be used to detect the variations of magnetic field. It is because the coupling between the fiber core mode and surface plasmon polariton (SPP) mode is changed by varying the refractive index of the analyte[11,12]. According to Sharma *et al.*, the gold layer and MF layer are covered on a silicon chip. It succeeds in the reliable detection of a magnetic field, which results from the resonant angular and the full width at half-maximum of the SPR both being varied by the applied magnetic field[13]. Ying *et al.* have simulated a magnetic field sensor with the sensitivity of 0.612°/mT. In the sensor, the surface plasmon wave (SPW) is excited at the interface of the gold dielectric by the Kretschmann prism configuration. As the detected material of the magnetic field, the MF photonic crystal is inserted into a glass slot[14]. But, the magnetic field sensor based on a silica chip or prism configuration has a large sensing area, and the environment easily affects the signal wavelength.

In this Letter, we have investigated an MF injected side-hole fiber sensor based on SPR. Within the fiber sensor, the two side holes are coated with a gold film, and the MF is full filled into both of the side holes. The full vector finite element method is used in order to analyze the transmission properties of the side-hole fiber SPR sensor. The side-hole fiber SPR magnetic field sensor can be optimized by discussing the influences of the radius of the side hole, the thickness of the metal, and the distance between the fiber core and the core of the side-hole on the fiber SPR sensor. When the applied magnetic field increases from 30 to 210.9 Oe, the magnetic field sensitivity of the side-hole fiber SPR sensor can reach to 1.063 nm/Oe, which is higher than the other reported magnetic field sensors, such as the multimode interference fiber sensor[8], the microfiber sensor[6,15], the Fabry–Perot (FP) interferometer sensor[16,17], and the fiber grating sensor[2,18].

Figure 1 is the cross section of the MF injected side-hole fiber SPR sensor. In the side-hole fiber, the gold films are

 

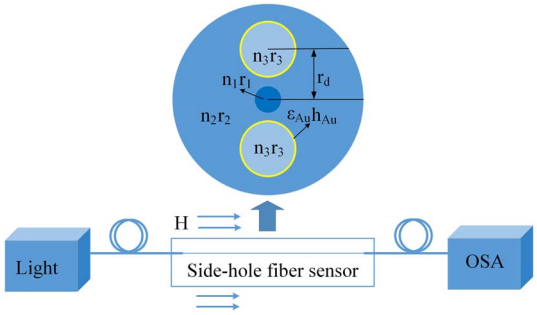


Fig. 1. Cross section of the side-hole fiber SPR sensor and the proposed setup for loss spectrum interrogation. OSA, optical spectrum analyzer.

deposited on the surface of the two side holes with the thickness of $h_{\mathrm{Au}}$. The distance between the fiber core and the core of the side hole is $r_d$, and the MF with the refractive index of $n_3$ is full filled into the two side holes. Moreover, the radiuses of the side-hole fiber are $r_1$ (fiber core), $r_2$ (fiber cladding), and $r_3$ (two side holes), respectively. The refractive index of the fiber core and cladding are $n_1 = 1.4814$, and $n_2 = 1.474$, respectively.

In the simulations, the Drude mode and Fresnel formula describe the complex dielectric constant of the gold film and the dispersion characteristics of pure silicon, respectively[19,20]. The coupling strength between the fiber core mode and the SPP mode is described by the confinement loss, which can be expressed as

$$\alpha_{\mathrm{Au}} = 8.686 \frac{2\pi}{\lambda} \mathrm{Im}(N_{\mathrm{eff}}), \tag{1}$$

where $\alpha_{\mathrm{Au}}$, $\mathrm{Im}(N_{\mathrm{eff}})$, and $\lambda$ are the confinement loss, the imaginary part of the effective refractive index of the fiber core, and the wavelength of the fiber sensor. As reported in Refs. [9,21], the refractive index of the MF with different external magnetic fields can be as shown in Table 1. From the data in Table 1, the initial refractive index of the MF is 1.462 (the concentration of the MF is 0.85 emu/g, and the applied magnetic field is 0 Oe) and remains constant until the external magnetic field is up to 30 Oe, then the refractive index of the MF increases as the external magnetic field increases from 30 to 210.9 Oe. The refractive index of the MF is varied as the external magnetic field changes, resulting in the resonant coupling between the fiber core mode and SPP mode taking place at other wavelengths.

Within the simulation model, the triangular subdomain is used to discretize the upper part of the fiber core, because the cross section of such a fiber sensor is longitudinally symmetrical. The mesh elements and freedom of degrees of the calculation area are 28317 and 197518, respectively. Moreover, the outermost layer is matched by the perfectly matched layer (PML), and the boundary condition of the horizontal boundary is assigned with the perfect electric conductor (PEC) artificial boundary condition. Figure 2 shows the field distribution of the upper part of the fiber core. In the side-hole fiber SPR sensor, the radius of the fiber core, cladding, and side hole are 4.15, 62.5, and 10 μm, respectively; the thickness of the gold is 45 nm, and the refractive index of the MF is 1.462. By comparing Figs. 2(a) and 2(b), it can be found that the field intensity at the interface of the gold MF of the $y$-polarized direction is much stronger than that of $x$-polarized direction, because the SPW is a TM-polarized wave. The SPR effect has no influence on the fiber core mode of the $x$-polarization.

**Table 1.** Refractive Index of the MF with Different External Magnetic Fields

| H (Oe) | 0 | 30 | 89.9 | 120.3 | 150 | 180.4 | 210.9 |
|---|---|---|---|---|---|---|---|
| $n_{\mathrm{MF}}$ | 1.462 | 1.462 | 1.4635 | 1.4645 | 1.4654 | 1.4662 | 1.4666 |

The real part of the refractive index of the fiber core mode of the $y$-polarization [$\mathrm{Re}(n_{\mathrm{eff}})$], that of the SPP mode [$\mathrm{Re}(n_{\mathrm{SPP}})$] and the loss spectrum, are shown in Fig. 3, when all parameters are the same as Fig. 2. From Fig. 3, the black and red solid lines represent the $\mathrm{Re}(n_{\mathrm{eff}})$ and $\mathrm{Re}(n_{\mathrm{SPP}})$, respectively. The $\mathrm{Re}(n_{\mathrm{eff}})$ is equal to the $\mathrm{Re}(n_{\mathrm{SPP}})$ at the wavelength of 1218 nm, where the loss increases to the maximum. It means that the fiber core mode of the $y$-polarization resonant couples into the SPP mode at the wavelength of 1218 nm, resulting in the loss reaching the maximum.

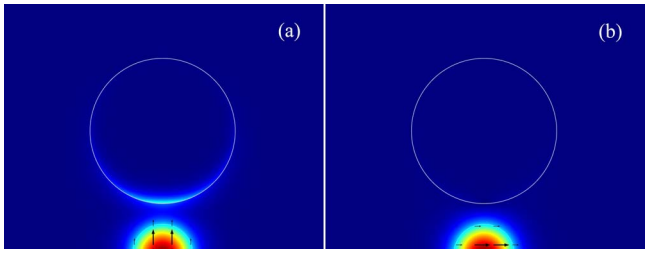


Fig. 2. Field distribution of the upper part of the fiber core of the (a) $y$-polarization and (b) $x$-polarization.

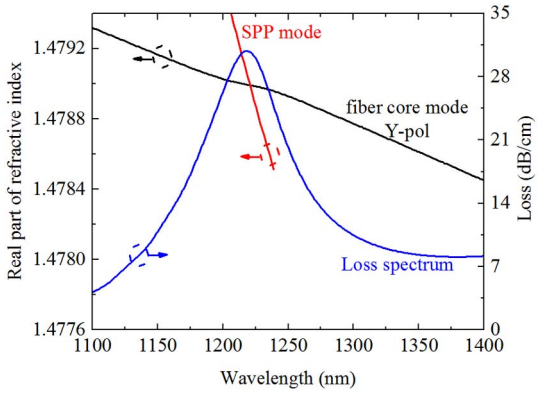


Fig. 3. $\mathrm{Re}(n_{\mathrm{eff}})$, $\mathrm{Re}(n_{\mathrm{SPP}})$, and the loss spectrum of the fiber sensor as a function of wavelength.

In the side-hole fiber SPR sensor, the main variables are the radius of the side hole, the distance between the side-hole core and the fiber core, and the thickness of the metal layer. Figure 4 is the loss spectrums with the different radiuses of the side hole, while the other parameters remain unchanged. As shown in Fig. 4, the peaking loss at the resonant wavelength of 1218 ($r_3 = 10$ μm), 1214 ($r_3 = 9$ μm), and 1207 nm ($r_3 = 8$ μm) are 30.846, 28.351, and 25.580 dB/cm, respectively. It illustrates that the peaking loss decreases, and the resonant wavelength moves to the shorter wavelength as the $r_3$ decreases. The bigger the radius of the side hole is, the more the MF is infected, leading to a larger influence on the SPW.

The distance between the fiber core and the core of the side hole is also discussed to optimize the side-hole fiber SPR sensor. Figure 5 plots the influence of $r_d$ on the loss spectrum, while other parameters remain unchanged. In the Fig. 5, the peaking loss is 17.598 dB/cm at the wavelength of 1219 nm when the $r_d$ is 17.35 μm, while the peaking loss increases to 30.846 dB/cm, and the resonant wavelength shifts to 1218 nm when the $r_d$ is 16.95 μm.

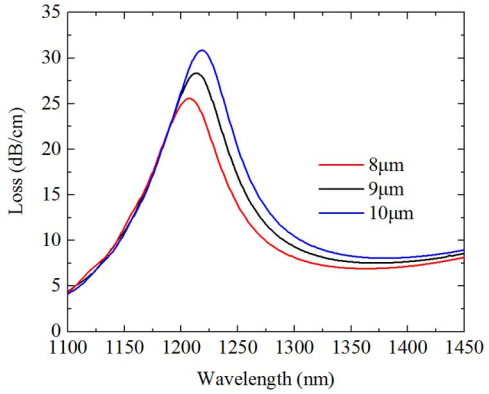


Fig. 4. Influence of $r_3$ on the loss spectrum of the side-hole fiber SPR sensor.

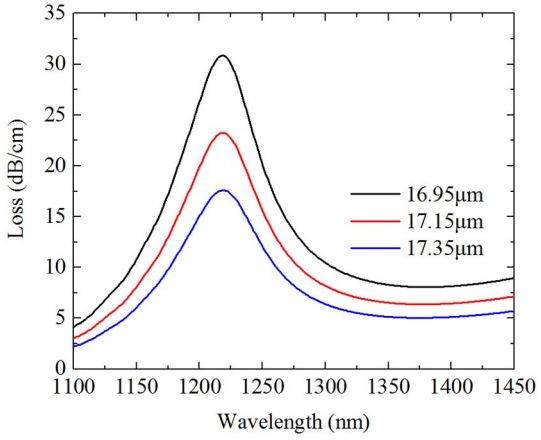


Fig. 5. Influence of $r_d$ on the loss spectrum of the side-hole fiber SPR sensor.

Therefore, the peaking loss decreases drastically, but the resonant wavelength has little change with the increasing of $r_d$. It is because the metal film is closer to the fiber core by decreasing the $r_d$, which influences the maximum achievable loss of resonance.

Furthermore, the resonant coupling between the fiber core mode and the SPP mode is sensitive to the thickness of the metal layer. Figure 6 illustrates the loss spectrums with different $h_{\mathrm{Au}}$, while other parameters of the side-hole fiber sensor based on SPR remain unchanged. In Fig. 6, the black, red, and blue solid lines represent the loss spectrums with $h_{\mathrm{Au}}$ of 45, 50, and 55 nm, respectively. From the loss spectrums in Fig. 6, the resonant wavelength shifts to a longer wavelength as the $h_{\mathrm{Au}}$ keeps increasing from 45 to 55 nm. Moreover, the peaking losses are 30.846 ($h_{\mathrm{Au}} = 45$ nm), 24.784 ($h_{\mathrm{Au}} = 50$ nm), and 19.118 dB/cm ($h_{\mathrm{Au}} = 55$ nm), respectively, which means the peaking loss decreases with the increasing of $h_{\mathrm{Au}}$.

The loss spectrums of the side-hole fiber SPR sensor with different external magnetic fields are plotted in Fig. 7(a), where $r_3$, $r_d$, and $h_{\mathrm{Au}}$ are 10 μm, 16.95 μm, and 45 nm, respectively, and the other parameters are unchanged. In this Letter, we set the range of the applied magnetic field as 30 to 210.9 Oe to analyze the sensing characteristic of the side-hole fiber SPR magnetic field sensor. When the external magnetic field is parallel to the side-hole fiber, as shown in Fig. 7(a), the loss spectrum of the side-hole fiber SPR sensor moves to a longer wavelength, and the peaking loss increases with the increasing of the external magnetic field. Assuming the resonant wavelength shift as $\Delta\lambda_{\mathrm{res}}$, the sensitivity of such fiber sensor is extracted by[22]

$$S = \frac{\Delta\lambda_{\mathrm{res}}}{\Delta H}\ (\mathrm{nm/Oe}), \tag{2}$$

where $\Delta H$ is the change of the external magnetic field. The resonant wavelength with different external magnetic fields are fitted and plotted in Fig. 7(b). It can be found that the values, which are plotted in Fig. 7(b) for the side-hole fiber SPR sensor, almost display a linear response.

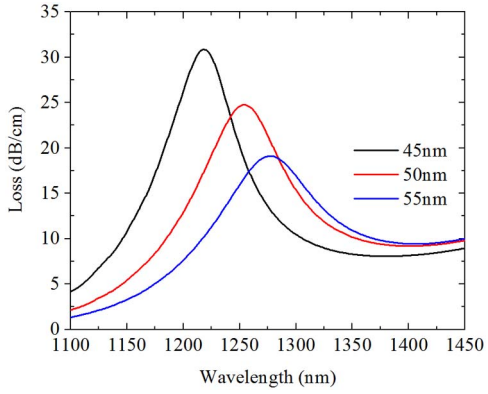


Fig. 6. Influence of $h_{\mathrm{Au}}$ on the loss spectrum of the side-hole fiber SPR sensor.

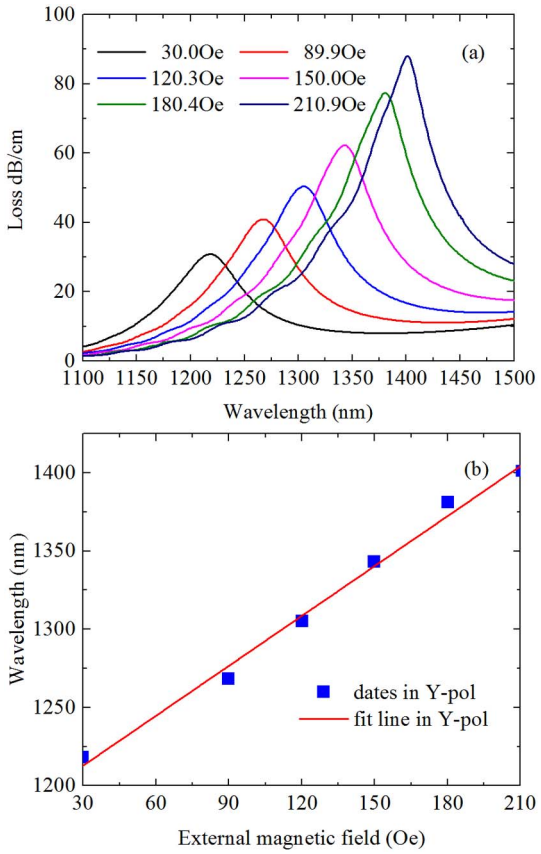


Fig. 7. (a) The loss spectrum with different external magnetic fields and (b) the fitted result of the resonant wavelength.

Furthermore, the sensitivity of the side-hole fiber SPR sensor can reach to 1.063 nm/Oe when the external magnetic field increases from 30 to 210.9 Oe.

In conclusion, we propose a side-hole fiber magnetic field sensor based on SPR. The gold film is deposited on the surface of two side holes to excite the SPR effect. The MF is full filled into two side holes, and the applied magnetic field is parallel to the side-hole fiber. By optimizing the side-hole fiber SPR sensor, the sensitivity can reach 1.063 nm/Oe when the external magnetic field is from 30 to 210.9 Oe. The research on the side-hole fiber sensor based on SPR would be very useful in the investigation of the detection of magnetic fields.

The work was supported by the National Natural Science Foundation of China under Grant No. 61525501.

## References

1. Y. Zheng, X. Dong, R. Yang, S. Zhang, J. C. C. Chan, and P. P. Shum, IEEE Sens. J. **14**, 3148 (2014).
2. L. Gao, T. Zhu, M. Deng, K. S. Chiang, X. Sun, X. Dong, and Y. Hou, IEEE Photon. J. **4**, 2095 (2012).
3. W. Lin, Y. Miao, H. Zhang, B. Liu, Y. Liu, and B. Song, Appl. Phys. Lett. **103**, 151101 (2013).
4. T. Hu, Y. Zhao, X. Li, J. Chen, and Z. Lv, Chin. Opt. Lett. **8**, 392 (2010).
5. H. Tian, C. Zhou, D. Fan, Y. Ou, and D. Yin, Chin. Opt. Lett. **12**, 24 (2014).
6. Y. Miao, J. Wu, W. Lin, K. Zhang, Y. Yuan, B. Song, H. Zhang, B. Liu, and J. Yao, Opt. Express **21**, 29914 (2013).
7. P. Zu, C. C. Chan, W. S. Lew, Y. Jin, Y. Zhang, H. F. Liew, L. H. Chen, W. C. Wong, and X. Dong, Opt. Lett. **37**, 398 (2012).
8. Y. Chen, Q. Han, T. Liu, X. Lan, and H. Xiao, Opt. Lett. **38**, 3999 (2013).
9. J. Li, R. Wang, J. Wang, B. Zhang, Z. Xu, and H. Wang, Opt. Fiber Technol. **20**, 100 (2014).
10. H. V. Thakur, S. M. Nalawade, S. Gupta, R. Kitture, and S. N. Kale, Appl. Phys. Lett. **99**, 161101 (2011).
11. W. Tsai, K. Lin, S. Yang, Y. Tsao, and P. Ho, Chin. Opt. Lett. **12**, 67 (2014).
12. B. Shuai, L. Xia, and D. Liu, Opt. Express **20**, 25858 (2012).
13. A. K. Sharma and T. Nagao, Appl. Phys. B Lasers Opt. **117**, 363 (2014).
14. Y. Ying, Y. Zhao, R. Lv, and H. Hu, IEEE Trans. Instrum. Meas. **65**, 1 (2015).
15. L. Luo, S. Pu, J. Tang, X. Zeng, and M. Lahoubi, Appl. Phys. Lett. **106**, 816 (2015).
16. Y. Zhao, R. Q. Lv, Y. Ying, and Q. Wang, Opt. Laser Technol. **44**, 899 (2012).
17. R. Q. Lv, Y. Zhao, D. Wang, and Q. Wang, IEEE Photon. Technol. Lett. **26**, 217 (2014).
18. J. Zheng, X. Dong, P. Zu, L.-Y. Shao, C. C. Chan, Y. Cui, and P. P. Shum, Opt. Express **21**, 17863 (2013).
19. A. Vial, A.-S. Grimault, D. Macías, D. Barchiesi, and M. L. de la Chapelle, Phys. Rev. B **71**, 085416 (2005).
20. G. Agrawal, "Nonlinear Fiber Optics," in *Nonlinear Science at the Dawn of the 21st Century*, P. L. Christiansen, M. P. Sørensen, and A. C. Scott, eds. (Springer, 2000), pp. 195.
21. Y. F. Chen, S. Y. Yang, W. S. Tse, H. E. Horng, C. Y. Hong, and H. C. Yang, Appl. Phys. Lett. **82**, 3481 (2003).
22. H. Chen, S. Li, J. Li, and Z. Fan, IEEE Photon. Technol. Lett. **27**, 1 (2015).